Active Layer Stratigraphy and Organic Layer Thickness at a Thermokarst Site in Arctic Alaska Identified Using Ground Penetrating Radar

Authors: Gusmeroli, Alessio, Liu, Lin, Schaefer, Kevin, Zhang, Tingjun, Schaefer, Timothy, et al.

Active layer stratigraphy and organic layer thickness at a thermokarst site in Arctic Alaska identified using ground penetrating radar

Alessio Gusmeroli[1]

Lin Liu[2,8]

Kevin Schaefer[3]

Tingjun Zhang[4]

Timothy Schaefer[5] and

Guido Grosse[6,7]

[1]International Arctic Research Center, University of Alaska Fairbanks, 930 Koyukuk Drive, Fairbanks, Alaska 99775, U.S.A.
[2]Earth System Science Programme, 315 Mong Man Wai, Faculty of Science, The Chinese University of Hong Kong, Shatin, N.T., Hong Kong
[3]National Snow and Ice Data Center, Cooperative Institute for Research in Environmental Sciences, 449 UCB, University of Colorado, Boulder, Colorado 80309, U.S.A.
[4]MOE Key Laboratory of Western China's Environmental System, College of Earth and Environmental Sciences, Lanzhou University, Lanzhou, 730000, China
[5]Galmont Consulting, 70 West Madison, Chicago, Illinois 60016, U.S.A.
[6]Geophysical Institute, University of Alaska Fairbanks, Fairbanks, Alaska 99775, U.S.A.
[7]Present address: Alfred Wegener Institute, Centre for Polar and Marine Research, Telegrafenberg A43, D-14473 Potsdam, Germany
[8]Corresponding author: liulin@cuhk.edu.hk

Abstract

In permafrost terrains, the frozen-unfrozen boundary, located at the base of the active layer, is a prominent ground-penetrating radar (GPR) target and is typically used to retrieve active layer thickness. Less attention has been given to the capability of the GPR in detecting structures within the active layer. In this paper, using 500 MHz GPR data from a thermokarst site in the Arctic Coastal Plain, we demonstrate that GPR can retrieve, when present, the internal stratigraphy of the thawed layer. We recognized two types of thermokarst-related microtopographic units: dry-and-uniform peaty hummocks with a thin (~30 cm) active layer and inter-hummock depressions with a thicker (~60 cm) active layer characterized by two different layers—a surface peat layer on top of silt confirmed by test pits. Radar wave velocity analysis, done with a common-midpoint survey, suggests a contrast in volumetric water content (87% and 45% for the upper and lower layers, respectively). The subsurface radar wave velocity suggests that the porous peat layer contains more water (87% by volume) than the underlying silt layer (45% by volume), resulting in a strong dielectric contrast and a strong radar reflection. This study demonstrates the usefulness of GPR to measure the thickness and properties of the surface organic layer in permafrost regions.

Introduction

The tundra biome covers vast areas of Alaska, Canada, and Siberia. The ground here is snow covered and frozen for much of the year, and biomass productivity is concentrated during the short, three-month summer. The maximum depth of seasonal thaw defines active layer thickness (ALT), a key parameter for ecosystems, biogeochemical cycling, and hydrology in high northern latitudes. ALT measurements are extremely important, as they provide the data needed to understand baseline conditions and to characterize changes in permafrost. The Circumpolar Active Layer Monitoring (CALM) network has been measuring ALT at 168 sites since the 1990s (Brown et al. 2000; Streletskiy et al., 2008; Shiklomanov et al., 2010). CALM measurements over the past two decades indicate that ALT has increased in Scandinavia, the Russian Arctic, and the interior of Alaska, though no trends were observed for the North American Arctic (AMAP, 2012). Field and remote sensing-based long-term observation of subsidence in the Arctic Coastal Plain indicate that melting of excess ice could explain the lack of a significant temporal trend in ALT (Streletskiy et al., 2008; Liu et al., 2010), even though permafrost temperatures show clear signs of warming (Smith et al., 2010).

ALT in Arctic Alaska is typically measured manually at the end of summer, using a steel probe to penetrate the thawed ground until it reaches the permafrost table. This manual method is simple and fast, but the data represent point measurements, which may be inadequate for characterizing spatial variability across the landscape. Ground-penetrating radar (GPR) in the 0.1–1.0 GHz frequency range offers a viable alternative to obtain spatially continuous estimates of ALT. Many studies have used GPR to map thaw depth at a variety of Arctic sites (Dolittle et al., 1990; Bradford et al., 2005; Brosten et al., 2006; Brosten et al., 2009; Hubbard et al., 2012); at mountainous sites with thick active layer and rocky soils, traditional steel probing is hard to implement and GPR represents a viable alternative for smooth ALT retrieval (Westermann et al., 2010; Wollschläger et al., 2010). GPR has also been used to monitor freeze and thaw processes in seasonally frozen ground (e.g., Steelman et al., 2010).

GPR consists of a radar transmitter and receiver mounted on a sled. The GPR transmits radar pulses into the ground and when the pulse reaches a boundary with different dielectric permittivity, part of the pulse is reflected back to the receiver. Because the dielectric permittivity of water is ~25 times greater than that of ice, the transition from unfrozen to frozen ground at the permafrost table produces a very clear radar reflection. The GPR records the travel time of this reflection and the depth to the permafrost table is calculated from an assumed or estimated radar velocity. Past studies using GPR to measure thaw depth all assumed a uniform, homogeneous active layer with a constant wave velocity.

Our GPR survey in August 2012 at an active thermokarst site on the North Slope of Alaska detected recognizable stratigraphy within the active layer consisting of an upper layer of peat and a lower layer of silt. We here report on the characteristics of this two-layer stratigraphy and discuss possible mechanisms causing its formation.

Field Area and Data Acquisition

We performed a GPR campaign on 16–19 August 2012 at a site near Prudhoe Bay in northern Alaska (Fig. 1). The study site was chosen because of the peculiar microgeomorphology, which clearly differs from the more typical ice-wedge polygon landscape of the surrounding tundra. Two prominent microtopographic units characterized the study area: small elevated hummocks (A in Fig. 1) and interhummock depressions (B in Fig. 1). The depressions were flat with up to 10 cm of standing water and young, relatively sparse sedges between 10 cm and 30 cm tall. The hummocks rose 30 cm to 80 cm above the depressions with rough, irregular surfaces, dense sedges and shrubs between 10 cm and 15 cm tall, and moist, but well-drained soils. The hummocks were irregular in shape with no obvious spatial pattern except a tendency to be longer in the natural direction of drainage, which at this site is from the southwest to the northeast.

We surveyed the field site using a 500 MHz PulseEkkoPro GPR system, which, for 0.04–0.05 m ns^{-1} radar wave velocity, has a radar wavelength of 8–10 cm capable of penetrating a few meters below the surface. For radar imaging, we used the common-offset (CO) survey mode, which means we kept the distance between transducers constant at 0.25 m during the entire survey. We towed the unit across the tundra on straight, closely spaced transects, running approximately parallel to each other, and collected a radar trace every 0.2 seconds. We georeferenced each GPR trace with GPS coordinates from a Garmin GPSMAP 60CSx Handheld GPS Navigator. We conducted one common midpoint (CMP) survey to estimate radar wave velocity and dielectric properties of the subsurface. During the CMP survey, we incrementally distanced the transmitting and the receiving antennas apart from a central point. The CMP step size was 0.04 m and the maximum offset covered was 1 m. The CMP was undertaken specifically to investigate the dielectric structure, a depression in which a two-layer GPR stratigraphy was observed. Over a 100-m-long profile, we also collected detailed data by mechanical probing with an active layer probe at 1 m interval along the profile. With this widely accepted field method we assume no penetration of the probe into the permafrost.

GPR Data Processing and CMP Radar Velocity Analysis

Processing of the CO and CMP surveys followed standard routines for GPR data, including dewow (a filter for removing low-frequency instrumental noise), background-re-

moval, Ormsby bandpass filter with four corner frequencies 125–500/1000–2000 MHz, and a time-scaled gain to correct for spreading losses. We picked time zero from raw data and reflection travel time in the processed images using a standard phase-following algorithm included in the ReflexW software (Sandmeier Software™). In the simplest case of thawed ground above permafrost, ALT can be calculated by multiplying the measured two-way travel time of the reflection (t, usually in nanoseconds) by the radar velocity in the active layer (v_{ALT}). We estimated v_{ALT} using direct comparison with the GPR surveys and probe data ($v_{ALT} = ALT \, t^{-1}$).

In the CMP data, the travel time t of the reflected energy may be approximated by the hyperbolic normal moveout (NMO) equation:

$$t(x) = \sqrt{t_0^2 + \frac{x^2}{V_{NMO}^2}} \qquad (1)$$

where x is the antenna offset, t_0 is the zero-offset travel time, and V_{NMO} is normal moveout velocity. For energy reflected from the horizontal base of a homogeneous, isotropic layer, Equation 1 is exact and V_{NMO} is radar wave velocity in the medium. For a multilayer case, refraction across interfaces introduces nonhyperbolic terms and Equation 1 is an approximation to actual data. For small velocity contrasts, isotropic layers and short-spread conditions (i.e., x is approximately equal to reflector depth z; Taner and Koehler, 1969), V_{NMO} is considered as the root-mean-square velocity (V_{RMS}), and medium velocity for each layer may be obtained by substituting V_{RMS} into Dix's equation (Dix, 1955). Here we estimate V_{NMO} using the coherence statistics (Sheriff and Geldart, 1995; Booth et al., 2010, 2011). Coherence is a measure of the coherency of energy between radar waveforms. We used the methods outlined by Booth et al. (2011) to correct a known systematic bias in V_{NMO} caused by the nature of radar waveforms.

Uncertainties in GPR measurements of ALT result from uncertainties in constraining the reflector travel times and uncertainties in the radar velocity. Both were determined from uncertainties in determining reflection travel times: 0.4 ns, or twice the system temporal sampling rates. We calculated and combined both uncertainties using formal error propagation (Topping, 1972).

Results

RADAR VELOCITY WITHIN THE SUBSURFACE

The CMP image (Fig. 2, part a), that is, a time versus antenna offset plot, shows at least four coherent waveform events:

1. The air wave that propagates between transmitter and receiver (blue circle in Fig. 2, part a). This air wave travels at the velocity of light in air (0.3 m ns^{-1}) and has a characteristic linear travel time (the arrival time linearly increases with increasing antenna separation).
2. The ground wave that couples with the ground surface immediately below the antennas (purple circle in Fig. 2, part a). The ground wave moveout (the increase of wave arrival time with increasing distance) is linear.
3. The first reflected wave (L1, red circle in Fig. 2, part a) with hyperbolic moveout starting at ~17 ns.
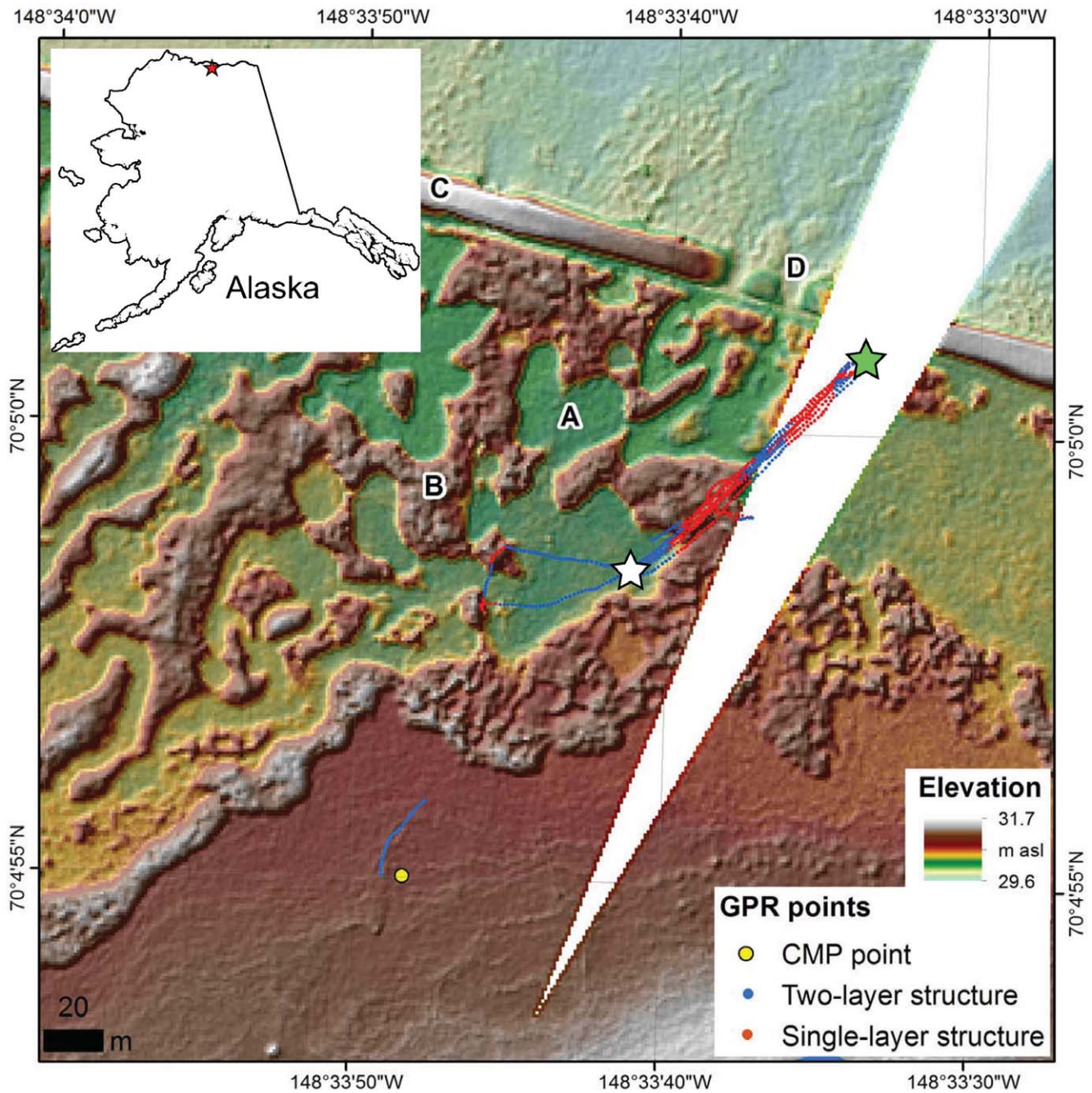
FIGURE 1. A 2011 LiDAR Digital Elevation Model of study site near Prudhoe Bay in northern Alaska with the ground penetrating radar (GPR) transects indicated as red and blue dots. White regions indicate missing LiDAR data. Label A indicates a wet depression, B is a dry hummock, with subsurface ice, C is the access road for the Trans-Alaska pipeline, and D is a spillover for flood prevention. Green and white stars indicate starting and ending points of the sample GPR image depicted in Figure 3, part a. The two layer stratigraphy (blue dots) only occurs in topographic depressions.

4. The second reflected wave (L2, green circle in Fig. 2, part a). This event is high in amplitude and becomes distinguishable at ~27 ns.

Of all these events, we seek to use the hyperbolic reflections to determine properties within the active layer. The coherence response of the CMP data shows two clusters corresponding to L1 and L2 (red and green circles in Fig. 2, part b). Coherence peaks

for the two events yielded $V_{\mathrm{NMO}} = 0.038 \pm 0.002$ and 0.043 ± 0.002 m ns^{-1}, respectively with uncertainty estimated at $\pm$ 50% of the coherence peak (Tronicke et al, 2000; Booth et al., 2010). The application of "backshifting," the correction described in Booth et al. (2010), resulted in slightly higher values that gave the final results of 0.039 ± 0.002 m ns^{-1} for the upper layer; 0.054 ± 0.002 m ns^{-1} for the lower layer and 0.045 ± 0.002 m ns^{-1} for the entire active layer column.
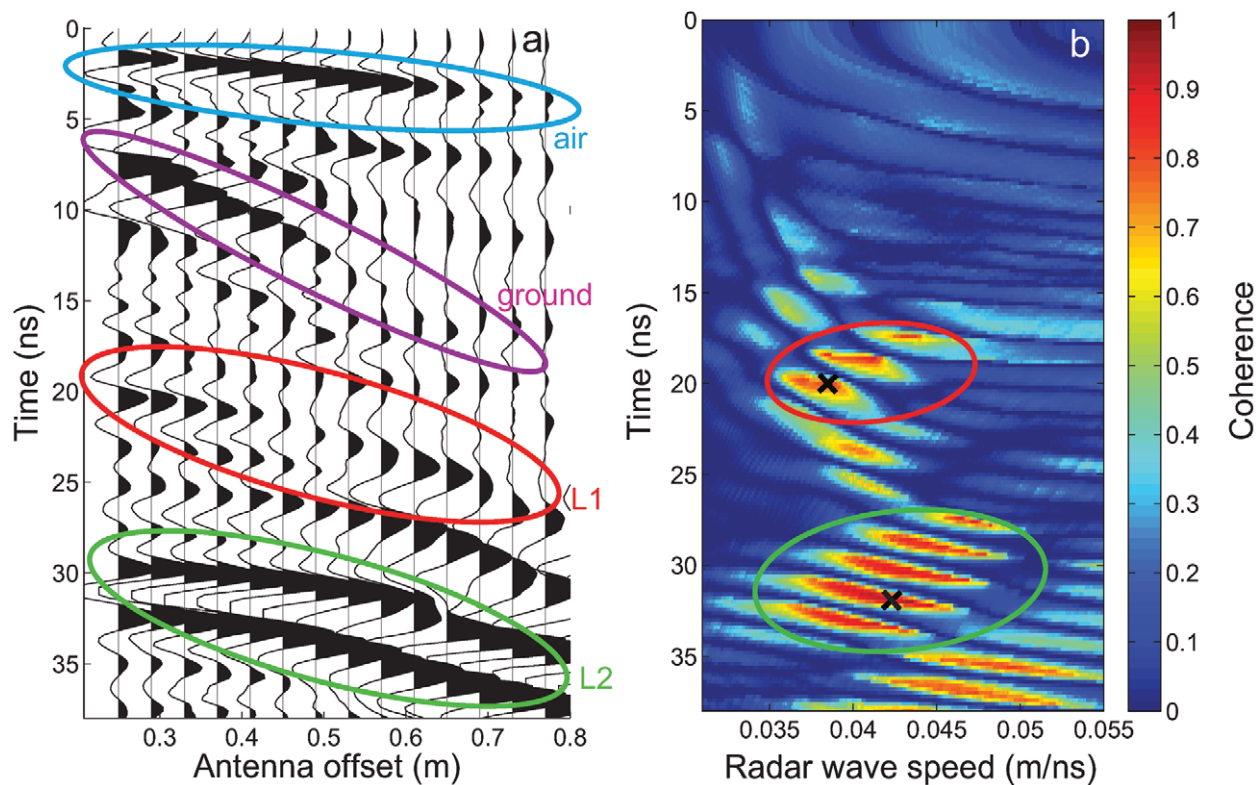
FIGURE 2. (a) The 500 MHz Common Mid Point gather and (b) coherence plot at our study site. The CMP gather (a) shows two coherent hyperbolic reflections: L1 (red) corresponds to the transition from peat to silt and L2 (green) corresponds to the permafrost table. Peaks in the coherence plot (crosses in b), allow normal-move-out velocity determination (Equation 1).

TWO-LAYER STRUCTURE IN GPR DATA

Figure 3 shows an example GPR image as a 100-m-long ra-dargram. This transect contains ~1300 data points with an along-track spatial resolution of 5–10 cm. The most prominent feature in our radar profiles is a spatially continuous, strong reflection from the permafrost table at the base of the active layer. This strong radar reflection results from the very high dielectric contrasts between the unfrozen soil and permafrost (51.0 for unfrozen ground and 3.2 for ground ice). A comparison between GPR-measured ALT and probe indicates a good agreement, in most of the cases within 5 cm (Fig. 4). The radar-characteristics of the active layer vary along the profiles. In some regions, the active layer appears uniform, with no recognizable returns within the active layer. In other regions, the GPR detected a reflection within the active layer. However, at 5, 40, and 90 m the return time sharply increased with a clear second reflection, indicating a deeper ALT with two distinct layers.

Discussion

The presence of two distinct layers occurred only in the de-pressions where the active layer was thicker. The elevated hum-mocks had a thin and uniform active layer (Fig. 5, part a, and '~5 m' and '~45 m' markers in Fig. 5, part b) whereas the depressions ('~15 m' and '~60 m' markers in Fig. 5, part b) had a thick and stratified active layer. A pit dug into one of the hummocks (Fig. 5, part c) revealed a uniform peat layer ~30 cm sitting on top of mas-sive ice. The radar reflected off the ice-rich layer, resulting in thin

clear recognition of thin active layers on the hummocks. A second pit dug through the active layer in one of the depressions showed two distinct, unfrozen layers (Fig. 5, part d): a dark, peat layer on top of a lighter layer of fine gray silt. The depressions where we detected the two-layer structures all had standing water, indicating fully saturated soils. Peat is more porous than silt, so the organic-rich top layer contained more water than the silt layer, resulting in a change in radar velocity at the interface between the two layers, and thus a radar reflection.

We hypothesized that radar reflectivity is caused by differ-ences in water content and between the peat and silt layers. This hypothesis was verified using radar wave velocities estimated in the CMP survey. Radar wave velocity in the top layer is lower than the deeper layer (0.039 and 0.054 m ns^{-1}, respectively). By assum-ing that both layers are fully saturated, we can use empirical rela-tions to estimate θ, the volumetric water content. For the upper peat we use the linear regression developed by Parsekian et al. (2011), whereas for the lower silt we use the mixing model of Greaves et al. (1996).

Using the measured values, we obtain θ = 87% and 45% for the peat layer and the silt, respectively, which are within the range of expectable values for saturated silt and peat (e.g., Davis and Annan, 1989). These differences in water content are sufficient to define a dielectric contrast that generates identifiable radar reflec-tions. The polarity of the reflections confirms our interpretation of a deeper layer with lower water content and higher dielectric constant. All reflectors in our radargrams show the same polarity (white-black-white), suggesting that the reflections are caused by a
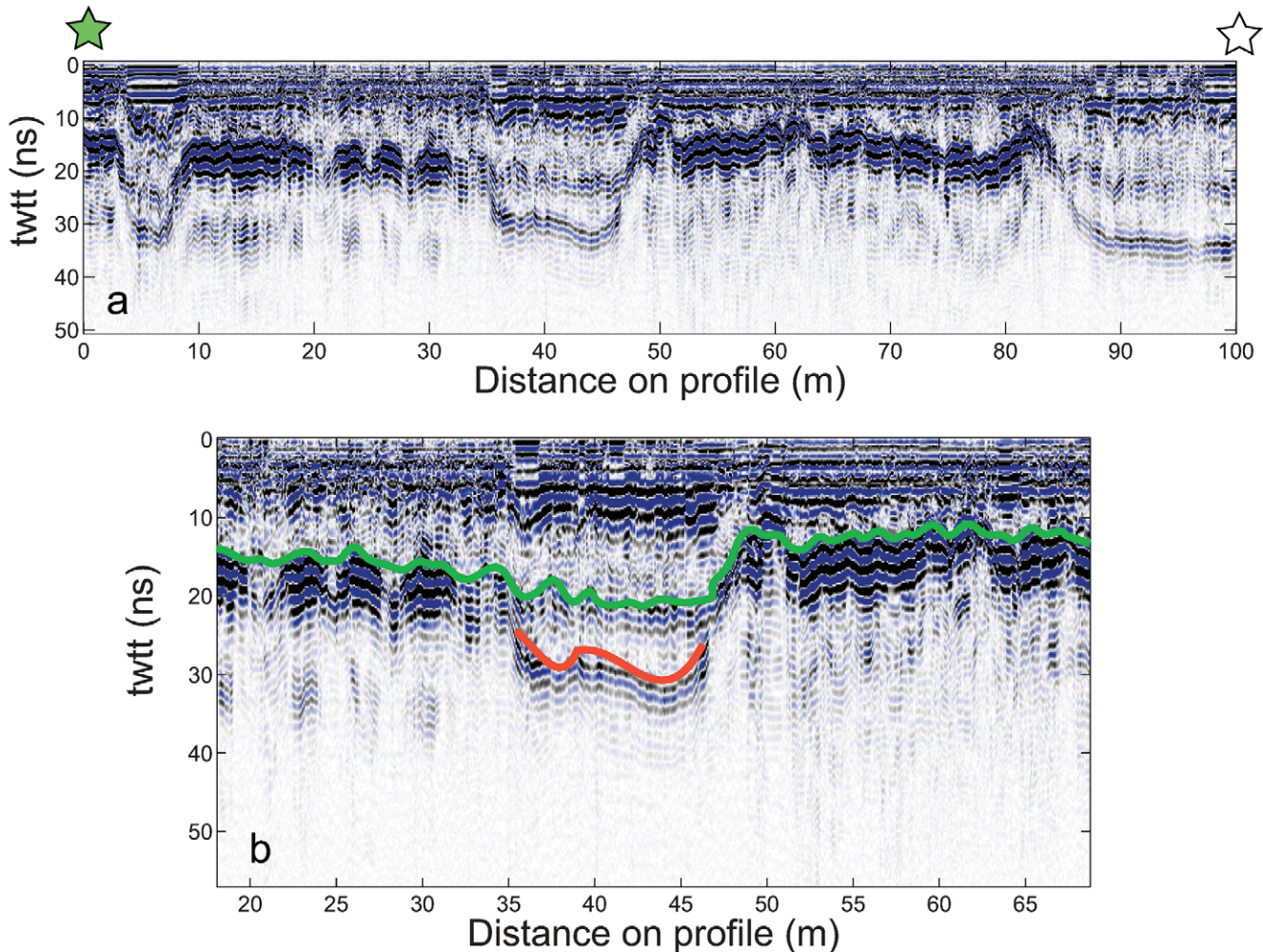
FIGURE 3. (a) An example of 500 MHz radar data acquired at our study site showing the two-way travel time (twtt) of the radar reflections as a function of distance. A two layer structure is visible at 5, 40, and 90 m on the profile. The stars indicate the start and end points shown in Figure 1. (b) Details of the radar stratigraphy in regions (18 m to 68 m along the profile) with a two-layer structure. The green line is the base of the peat layer; the red line is the silt-permafrost boundary.
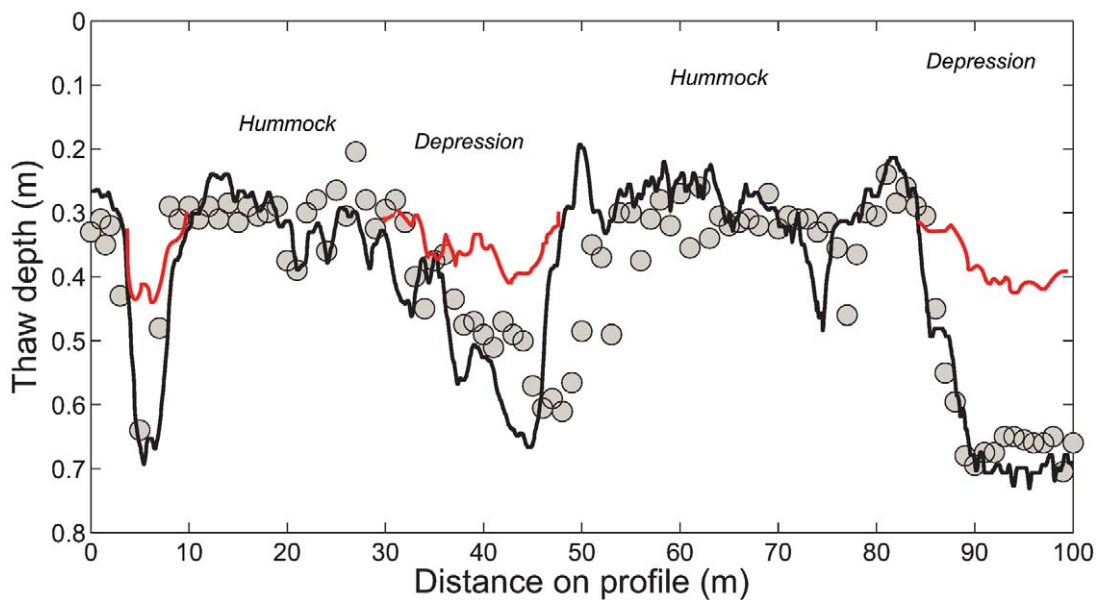

FIGURE 4. Comparison of thaw depth results between GPR (black line) and probing (circles) along one transect. The red line indicates organic layer thickness measured with the GPR. The radar speed of 0.045 m ns⁻¹, measured with the CMP, was used to convert GPR travel time into thaw depth estimates.
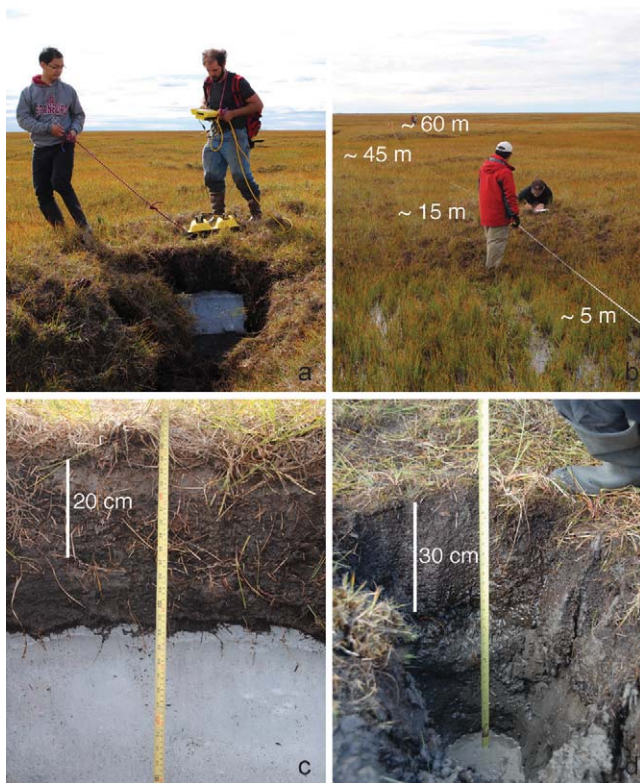
ALESSIO GUSMEROLI ET AL. / 199

FIGURE 5. Photographs of the study area with variable active layer and permafrost conditions. (a) Researchers pulling the GPR unit over a test pit on a hummock. (b) Researchers recording vegetation conditions along the survey line showing approximate distances corresponding to hummocks and depressions in Figures 3 and 4. (c) A test pit on a hummock showing an ~30 cm organic layer on top of ice. (d) A test pit in a depression showing a 30 cm organic layer on top of fine gray silt.

contrast of higher dielectric permittivity on top of lower dielectric permittivity.

The complicated microtopography of hummocks and depressions at this site likely resulted from thermokarst activity triggered by the building of the pipeline access road. A sequence of historical images of the study site (Fig. 6) suggests that geomorphic changes linked to thermokarst development started between 1979 and 1988, after road construction, and clearly expanded between 1988 and 2006. After initial construction, the road dammed the northward flow of surface water, creating a lake that eventually breached parts of the road. The road was rebuilt with spillovers to minimize flooding, but standing water still tended to accumulate south of the road.

The standing water triggered thawing of the upper portion of the underlying, ice-rich permafrost, which, after the excess ice melted out, caused the ground to subside (Fig. 7). The subsidence allowed more standing water to accumulate and the thermokarst zone expanded southward and eastward. The historical images in Fig. 6 suggest that the hummocks formed after the thermokarst subsidence as ice layers developed and heaved up the surface peat layer, although a detailed analysis of this process is out of the scope of this paper.

The two-layer structure we detected in the depressions consisted of the original surface peat layer on top of recently thawed

silt with all excess ground ice melted and drained away. The subsidence did not induce much erosion due to the flatness of the site, so the peat layer was preserved with minimal disturbance. The average thickness of the peat layer was 30 cm, which was typical of this region (Johnson et al., 2013). Sample pits dug north of the access road indicate that before the road was built, this site likely had a peat layer sitting on top of ice-rich, frozen silt. When the ice-rich silt thawed, the ground subsided and collected water, resulting in a fully saturated peat layer on top of a layer of thawed fine silt. The hummocks formed after the ground subsided when ice segregation at the silt boundary pushed up the peat layer, forming shallow sinuous ridges roughly parallel to the normal northeast flow of surface water. This terrain differs from what would typically result from melting ice wedges, where the melting of ice wedges and subsequent soil collapse tends to leave mounds at the polygon centers. The arrangement of such mounds would reflect the original polygon structure and the mounds themselves are typically not underlain by ice.

The thickness of the organic layer is crucial to the formation of permafrost. It is believed to control future permafrost degradation under warming climate (Yi et al., 2007) and strongly influences the temperature regime of the underlying permafrost (Johnson et al., 2013). GPR has been used to measure the thickness of the organic layer in permafrost regions, but typically in peat bogs with floating vegetation mats (e.g., Parsekian et al., 2011). Currently, the only way to measure the organic layer thickness is to dig a test pit and measure it. Here we find that under saturated conditions with a well-defined organic horizon, we can use GPR to measure the organic layer thickness. This opens up the possibility of greatly increasing the number of measurements of organic layer thickness over larger areas and different terrains.

Conclusions

Using GPR, we detected a distinct, two-layer stratigraphy within the active layer in local depressions at a site on the North Slope of Alaska undergoing geomorphological change as a result of thermokarst expansion. Our results demonstrate that active layer properties can be both spatially and vertically heterogeneous. At this site, a small pipeline access road blocked the normal drainage of water, which triggered water pooling and thawing of the upper portion of the ice-rich permafrost common to this region. The ground subsided, forming a series of water-filled depressions and ice-filled hummocks. The hummocks showed a thin (~0.3 m) peat layer directly on top of a layer of ground ice. The depressions showed standing water and a distinct double layer consisting of a peat layer with ~87% porosity and a deeper layer of thawed silt with ~45% porosity. The difference in water content between the peat and silt layers resulted in a strong dielectric contrast and a clear radar reflection. This contrasts with other thaw depth surveys using GPR, where the only retrievable radar echo was the reflection from the boundary between the frozen and unfrozen soil, and demonstrates the usefulness of GPR to measure the thickness of the organic layer.
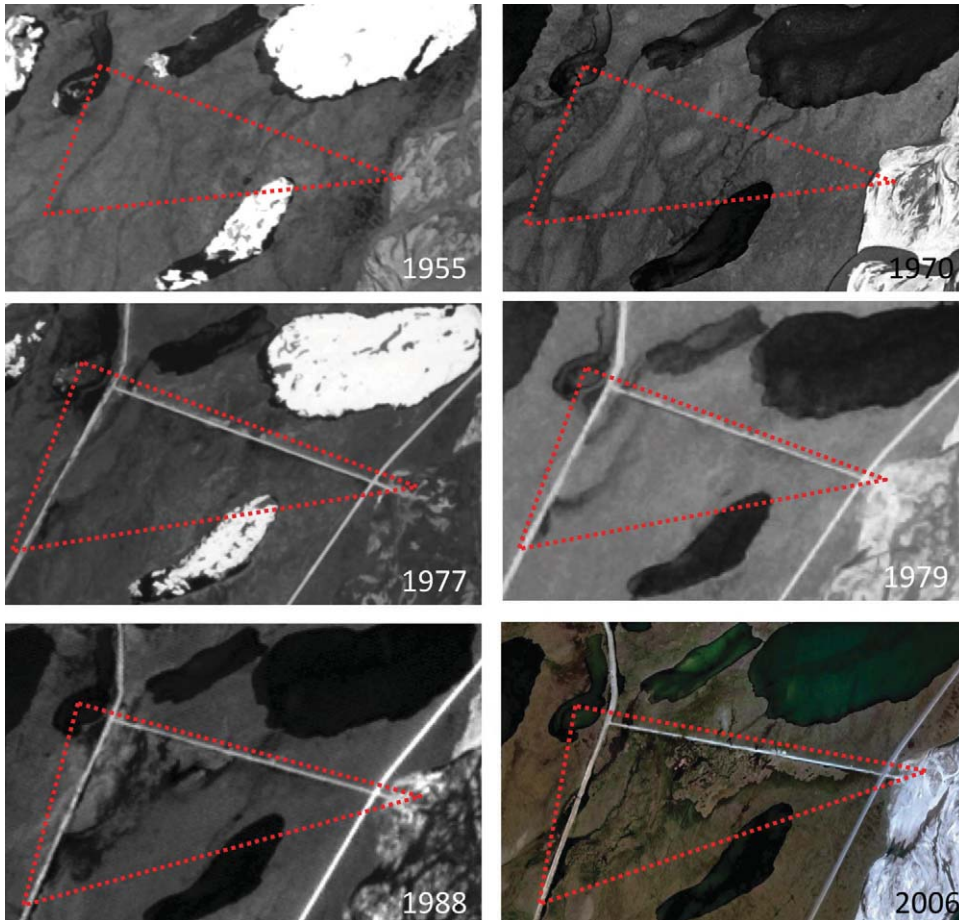
Acknowledgments

FIGURE 6. Historical satellite and aerial images indicate the site was stable until 1979. The 1988 SPOT image suggests that thermokarst development began between 1979 and 1988 and clearly expanded between 1988 and 2006. The drainage at the site originally was from lower left (SW) to upper right (NE) in the image, and the small access road built in the mid 1970s blocked this natural drainage.
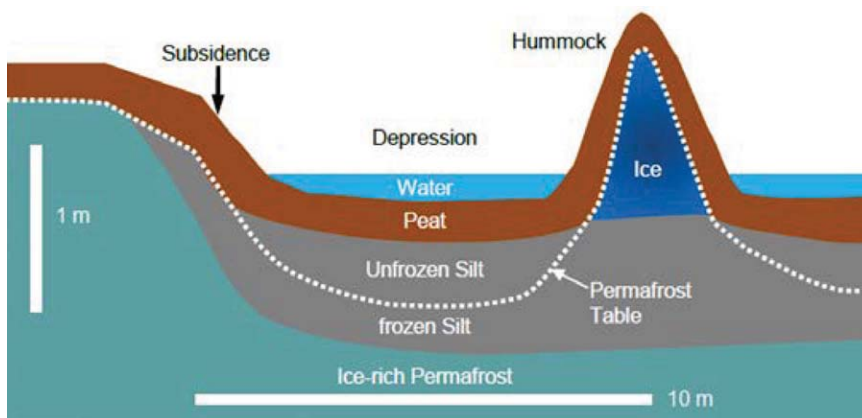
FIGURE 7. Schematic of subsurface structure at the study site. The thawing of ice-rich permafrost at the site produces large-scale subsidence, resulting in a series of depressions filled with water and small hummocks heaved up by ice. The secondary reflection detected in the depressions by the GPR is the boundary between the peat and the underlying silt.

ALESSIO GUSMEROLI ET AL. / 201

Booth kindly provided the script to analyze the CMP as well as numerous helpful suggestions.

References Cited

AMAP, 2012: *Arctic Climate 2011: Snow, Water, Ice and Permafrost in the Arctic (SWIPA)*. Oslo, Norway: Arctic Monitoring and Assessment Programme.

Booth, A. D., Clark R. A., and Murray, T., 2010: Semblance response to a ground-penetrating radar wavelet and resulting errors in velocity analysis. *Near Surface Geophysics,* 8: 235–246.

Booth, A. D., Clark R. A., and Murray, T., 2011: Influences on the resolution of GPR velocity analyses and a Monte Carlo simulation for establishing velocity precision. *Near Surface Geophysics*, 9: 399–411.

Bradford, J. H., McNamara J. P., Boden W., and Gooseff, M. N., 2005: Measuring thaw depth beneath peat-lined Arctic streams using ground-penetrating radar. *Hydrological Processes*, 19: 2689–2699.

Brosten, T. R., Bradford, J. H., McNamara, J. P., Zarnetske J. P., Gooseff, M. N., Breck Bowden, W., 2006: Profiles of temporal thaw depths between two Arctic stream types using ground penetrating radar. *Permafrost and Periglacial Processes,* 17: 341–355.

Brosten, T. R., Bradford, J. H., McNamara, J. P., Gooseff, M. N., Zarnetske, J. P., Bowden, W. B., and Johnston, M. E., 2009: Estimating 3D variation in active layer thickness beneath Arctic streams using ground penetrating radar. *Journal of Hydrology,* 373: 479–486.

Brown, J., Hinkel, K. M., and Nelson, F. E., 2000: The circumpolar active layer monitoring (CALM) program: Research designs and initial results. *Polar Geography,* 24(3): 166–258, http://dx.doi.org/10.1080/10889370009377698.

Davis, J. L., and Annan, A. P., 1989: Ground-penetrating radar for high-resolution mapping of soil and rock stratigraphy. *Geophysical Prospecting,* 37: 531–551.

Dix, C. H., 1955: Seismic velocities from surface measurements. *Geophysics*, **20**: 68–86.

Dolittle, J. A., Hardisky, M. A., and Gross, M. F., 1990: A ground penetrating radar study of active layer thickness in areas of moist sedge and wet sedge tundra near Bethel, Alaska, U.S.A. *Arctic and Alpine Research,* 22(2): 175–182.

Greaves, R. J., Lesmes, D. P., Lee, J. M., and Toksoz, M. N., 1996: Velocity variation and water content estimated from multi-offset, ground penetrating radar. *Geophysics,* 61: 683–695.

Hubbard, S. S., Gangodagamage, C., Dafflon, B., Wainwright, H., Peterson, J., Gusmeroli, A., Ulrich, C., Wu, Y., Wilson, C., Rowland, J., Tweedie, C., and Wullschleger, S. D., 2012: Quantifying and relating land-surface and subsurface variability in permafrost environments using LiDAR and surface geophysical datasets. *Hydrogeology Journal,* 21 (1): 149–169.

Johnson, K. D., Harden, J. W., McGuire, A. D., Clark, M., Yuan, F., and Finley, A. O., 2013: Permafrost and organic layer interactions over a climate gradient in a discontinuous permafrost zone. *Environmental Research Letters,* 8: 12 pp., http://dx.doi.org/10.1088/1748-9326/8/3/035028.

Liu, L., Zhang, T., and Wahr, J., 2010: InSAR measurements of surface deformation over permafrost on the North Slope of Alaska. *Journal of Geophysical Research: Earth Sciences,* 115: F03023, http://dx.doi.org/10.1029/2009JF001547.

Parsekian, A. D., Jones, B. M., Jones, M. C., Grosse, G., Walter Anthony, K. M., and Slater, L., 2011: Expansion rate and geometry of floating vegetation mats on the margins of thermokarst lakes, northern Seward Peninsula, Alaska, USA. *Earth Surface Processes and Landforms,* 36(14): 1889–1897, http://dx.doi.org/10.1002/esp.2210.

Sheriff, R. E., and Geldart, L. P., 1995: *Exploration Seismology*. New York: Cambridge University Press.

Shiklomanov, N. I., Streletskiy, D. A., Nelson, F. E., Hollister, R. D., Romanovsky, V. E., Tweedie, C. E., and Brown, J., 2010: Decadal variations of active- layer thickness in moisture controlled landscapes, Barrow, Alaska: *Journal of Geophysical Research,* 115: G00I04, http://dx.doi.org/10.1029/2009JG00124.

Smith, S. L., Romanovsky, V. E., Lewkowicz, A. G., Burn, C. R., Allard, M., Clow, G. D., Yoshikawa, K., and Throop, J., 2010: Thermal state of permafrost in North America: a contribution to the international polar year. *Permafrost and Periglacial Processes*, 21(2): 117–135.

Steelman, C. M., Endres, A. L., and van der Kruk, J., 2010: Field observations of shallow freeze and thaw processes using high-frequency ground-penetrating radar. *Hydrological Processes*, 24: 2022–2033, http://dx.doi.org/10.1002/hyp.7688.

Streletskiy, D., Shiklomanov, N., Nelson, F., and Klene, A., 2008: Long-term active and ground surface temperature trends: 13 years of observations at Alaskan CALM sites. *In* Proceedings, Ninth International Conference on Permafrost, vol. 29, 1727–1732.

Taner, M. T., and Koehler, F., 1969: Velocity spectra—digital computer derivation and applications of velocity functions. *Geophysics,* 34: 859–881.

Topping, J., 1972: *Errors Observation and Their Treatment*. London: Chapman and Hall.

Tronicke, J., Dietrich, P., and Appel, E., 2000: Georadar velocity determination: A comparison of different techniques. *In* Proceedings, 6th meeting of the EEGS-ES, Bochum, Germany.

Westermann, S., Wollschläger, U., and Boike, J., 2010: Monitoring of active layer dynamics at a permafrost site on Svalbard using multi-channel ground-penetrating radar. *The Cryosphere,* 4: 475–487, http://dx.doi.org/10.5194/tc-4-475-2010.

Wollschläger, U., Gerhards, H., Yu, Q., and Roth, K., 2010: Multi channel ground-penetrating radar to explore spatial variations in thaw depth and moisture content in the active layer of a permafrost site. *The Cryosphere,* 4: 269–283, http://dx.doi.org/10.5194/tc-4-269-2010.

Yi, S., Woo, M. K., and Arain, M. A., 2007: Impacts of peat and vegetation on permafrost degradation under climate warming. *Geophysical Research Letters,* 34: L16504, http://dx.doi.org/10.1029/2007GL030550.